Performance Analysis on Interference and Frequency-to-Time Mapping Based Frequency Hopping Receiver

Yiwei Sun, Jingbo Li, Jianping Chen, and Guiling Wu, *Member, IEEE*

***Abstract*—The receiving performance of a frequency hopping receiver based on interference and frequency-to-time mapping are analyzed. The broadening of the receiving passband induced by high frequency hopping speed is theoretically analyzed. The spurious-free dynamic range (SFDR), the frequency-dependent RF gain, and the average signal-to-noise ratio (SNR) corresponding to the RF gain are theoretically derived to indicate the receiving performance. Experimental verifications on the SFDR and RF gain were conducted. The SFDR of the passband at 7.21 GHz is 77.23 dBc, and for the passbands located from 7 GHz to 23 GHz, the SFDR variance is below 3.2 dB, which fits well with the simulated results with the difference of less than 3.7 dB. The RF gain for passbands located from 2.6 GHz to 40.9 GHz were tested, and the difference is less than 2 dB compared to the theoretical results.**

***Index Terms*—Average signal-to-noise ratio, frequency hopping receiving, hopping speed, receiving gain, spurious-free dynamic range.**

I. Introduction

With the communication spectrum becoming more and more crowded, secure communications that avoid interference and interception have become a heated topic recently. Frequency hopping is one of the promising solutions for communication in complicated and hostile environment since it provides high anti-jamming and anti-interception performance by changing the carrier frequency rapidly within a large frequency range [1], [2]. By increasing the frequency hopping speed, the follower jammers have lower detection probability and are unable to block/intercept the communication. By increasing the frequency hopping range, the broadband interference that entirely blocks certain frequency bands can be avoided since the communications can select other frequency channels. Recently, a fast and large-range frequency hopping receiver based on interference and frequency-to-time mapping has been proposed [2]. After frequency hopping synchronization, the transmitted frequency hopping signals can be received and digitized by the proposed scheme, and the original transmitted binary codes can be recovered through demodulation and other signal procession in the digital domain afterwards. Benefited from the large working bandwidth of the Mach-Zehnder modulator (MZM) and the high switching speed of optical switches, the impulse response of the receiver can be tuned within the working bandwidth of MZM rapidly. Thus, it can receive high-speed and large-range frequency hopping signals. The number of receiving frequency and receiving selectivity were investigated in the previous work to illustrate the high anti-jamming and anti-interference abilities of the proposed receiver. To evaluate the receiving performance of the proposed frequency hopping receiver, other significant receiving performances are analyzed in this paper. For frequency hopping receivers, the hopping speed is one of the key characteristics since it is relevant to the anti-jamming and anti-interception performance. For analog receivers, the receiving linearity [4], [5], [6], [7], [8] and the receiving radio frequency (RF) gain [9], [10], [11], [12] are two important characteristics since they indicate the quality of the received signals by affecting the average signal-to-noise ratio (SNR). For the average SNR of the frequency hopping receiver, a time window with fixed duration should be chosen, because the receiving RF gain varies in different frequencies, and it affects the average SNR.

The paper is organized as follows. The hopping speed, the receiving linearity, the RF gain, and the average SNR are theoretically analyzed in Section II. In Section III, the analyses on the receiving linearity and the RF gain are verified in experiments. The conclusion is presented in Section IV.

II. Theoretical Analysis

The schematic of the proposed frequency hopping receiver based on interference and frequency-to-time mapping is shown in Fig. 1.

The optical pulses generated by the mode-locked laser (MLL) are shaped by the frequency tuning module composed by adjustable optical interference arms for optical spectrum shaping, and single mode fibers (SMFs) for frequency-to-time mapping The optical pulses after interference can be expressed

Manuscript received 25 October 2022; revised 18 January 2023; accepted 27 January 2023. Date of publication 31 January 2023; date of current version 13 February 2023. This work was supported by the National Natural Science Foundation of China (NSFC) under Grant 61627817. *(Corresponding author: Guiling Wu.)*

Yiwei Sun is with the State Key Laboratory of Advanced Optical Communication Systems and Networks, Shanghai Institute for Advanced Communication and Data Science, Department of Electronic Engineering, Shanghai Jiao Tong University, Shanghai 200240, China, and also with the China Academy of Space Technology, Xi'an 710110, China (e-mail: yiwei.sun@sjtu.edu.cn).

Jingbo Li, Jianping Chen, and Guiling Wu are with the State Key Laboratory of Advanced Optical Communication Systems and Networks, Shanghai Institute for Advanced Communication and Data Science, Department of Electronic Engineering, Shanghai Jiao Tong University, Shanghai 200240, China (e-mail: peter552@sjtu.edu.cn; jpchen62@sjtu.edu.cn; wuguiling@sjtu.edu.cn).

Digital Object Identifier 10.1109/JPHOT.2023.3240819

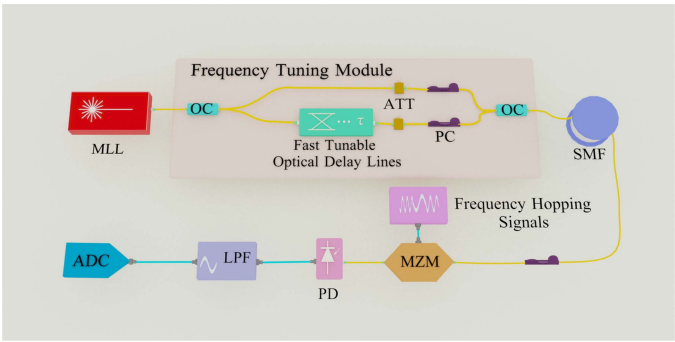

Fig. 1. The schematic of the proposed frequency hopping receiver based on interference and frequency-to-time mapping. MLL: mode-locked laser; OC:optical coupler; ATT: attenuator; PC: polarization controller; SMF: single mode fiber; MZM: Mach-zehnder modulator; PD: photodiode; LPF: low-pass-filter; ADC: analog-to-digital convertor.

as [12], [3]

$$I(\omega) = G(\omega) \cdot \left[2I_0 + 2I_0 \cdot \alpha \cdot \cos\left(\omega\tau\right)\right], \tag{1}$$

where $G(\omega)$ is the spectral profile of the MLL, τ is the time difference between the interference arms, I_0 is the optical power within each interference arm, and α is the visibility of the spectral interference. The attenuators (ATTs) and the polarization controllers (PCs) are used to maximize α, since the visibility of interference reaches its maximum with identical power and polarization state within the two interference arms [13]. The frequency-to-time mapping is conducted by a single mode fiber with the dispersion value of $\ddot{\Phi}_\nu$ [14]. The shaped optical pulses train, denoted as $p_{\mathrm{s}}(t)$, can be expressed as

$$\begin{aligned} p_{\mathrm{s}}(t) &= \sum_{n=0}^{\infty} p_{\mathrm{s,n}}(t - nT_{\mathrm{s}}), \\ p_{\mathrm{s,n}}(t) &= \exp\left(-\frac{jt^2}{2\ddot{\Phi}_\nu}\right) \cdot I(\omega)\Big|_{\omega=\frac{t}{\ddot{\Phi}_\nu}} \\ &= G\left(\frac{t}{\ddot{\Phi}_\nu}\right) \cdot \exp\left(-\frac{jt^2}{2\ddot{\Phi}_\nu}\right) \cdot 2I_0 \cdot \left[1 + \alpha \cdot \cos\frac{\tau}{\ddot{\Phi}_\nu}t\right]. \end{aligned} \tag{2}$$

Then the shaped optical pulses are modulated by the receiving frequency hopping signals in the MZM. After detected by the photo-diode (PD), anti-aliasing filtered by a low-pass filter (LPF) and digitized by the analog-to-digital converter (ADC) whose sampling rate is equal to the repetition rate of the MLL, the frequency hopping signals are digitized and filtered by the equivalent system response [15], [16]. If the MZM is working on the small signal condition and biased at the quadrature point, its impulse response, $h_{\mathrm{M}}(t)$, can be regarded as a cascade linear and time-invariant system in the equivalent system response [17], [18]. Therefore the equivalent system response, $h_{\mathrm{A}}(t)$, is proportional to the product of $p_{\mathrm{s}}(t)$ and $h_{\mathrm{E}}(t)$, the impulse response of the electric end including all the devices from PD to ADC [17]. With (2), $h_{\mathrm{A}}(t)$ can be expressed as

$$\begin{aligned} h_{\mathrm{A}}(t) &= h_{\mathrm{M}}(t) * \left[h_{\mathrm{E}}(t) \cdot p_{\mathrm{s}}(-t)\right] \\ &= h_{\mathrm{M}}(t) * \{h_{\mathrm{E}}(t) \cdot \\ &\left\{\sum_{n=0}^{N-1} G\left(\frac{t - nT_{\mathrm{s}}}{\ddot{\Phi}_\nu}\right) \cdot \exp\left[\frac{j(t - nT_{\mathrm{s}})^2}{2\ddot{\Phi}_\nu}\right] \cdot \right. \\ &\left.\left[2I_0 + 2I_0 \cdot \alpha \cdot \cos\left(\tau \cdot \frac{t - nT_{\mathrm{s}}}{\ddot{\Phi}_\nu}\right)\right]\right\}\Big\}. \end{aligned} \tag{3}$$

By rapidly tuning τ, the time difference between interference arms, $p_{\mathrm{s}}(t)$ is changed, and the receiving frequency of the equivalent system response, $\frac{\tau}{\ddot{\Phi}_\nu}$ changes consequently [3]. Thus, the frequency hopping signals can be received as the equivalent system response changes its receiving frequency according to the frequency hopping pattern.

A. Frequency Hopping Speed

The upper limit of the frequency hopping speed is determined by the tuning speed of the shaped optical pulses and the time to rebuild the equivalent system response. The time to tune the shaped optical pulses, as illustrated in Fig. 1, is determined by the switching time of the optical switches in the interference arms. Currently, the switching time of commercial optical switches is less than 10 ns. The requirement on the time to rebuild a stable equivalent system response is analyzed in this section.

Suppose the frequency hopping signal hops every $N \times T_{\mathrm{s}}$, where T_{s} is the sampling period of the ADC and it equals the period of the MLL. Then the frequency response of the equivalent system is the Fourier transform of the impulse response in (3) [15], and it can be derived as

$$\begin{aligned} H_{\mathrm{A}}(\omega) &= H_{\mathrm{M}}(\omega) \cdot \left[H_{\mathrm{E}}(\omega) * P_{\mathrm{s}}(\omega)\right] \\ &= H_{\mathrm{M}}(\omega) \cdot \left[H_{\mathrm{A},0}(\omega) * \delta(\omega) + \alpha H_{\mathrm{A},0}(\omega) * \delta\left(\omega - \frac{\tau}{\ddot{\Phi}_\nu}\right)\right], \\ H_{\mathrm{A},0}(\omega) &= 2I_0 \cdot H_{\mathrm{E}}(\omega) * \sum_{n=0}^{N-1} \left[e^{-jnT_{\mathrm{s}}\cdot\omega} \cdot G'(\omega)\right], \end{aligned} \tag{4}$$

where $P_{\mathrm{s}}(\omega)$, $H_{\mathrm{E}}(\omega)$ and $G'(\omega)$ are the Fourier transform of $p_{\mathrm{s}}(t)$, $h_{\mathrm{E}}(t)$ and $G(\frac{t}{\ddot{\Phi}_\nu}) \cdot \exp\left[\frac{j(t)^2}{2\ddot{\Phi}_\nu}\right]$, respectively. After frequency-to-time mapping, $G(\frac{t}{\ddot{\Phi}_\nu})$ is broadened in time domain, and its spectrum $|G'(\omega)|$ is narrowed in frequency domain with the bandwidth of no larger than few gigahertz. Therefore, $H_{\mathrm{A},0}(\omega)$ occupies the bandwidth of less than few gigahertz. Since $\omega = \frac{\tau}{\ddot{\Phi}_\nu}$ is designed for the reception of the frequency hopping signals transmitting at higher frequency bands, usually larger than ten gigahertz, the two receiving bands at $\omega = 0$ and $\omega = \frac{\tau}{\ddot{\Phi}_\nu}$, as in the square braces in (4) doesn't overlap. Thus, the equivalent system frequency response can be regarded as two passpands with identical profile, determined by $H_{\mathrm{A},0}(\omega)$, and different central frequencies at DC and $\omega = \frac{\tau}{\ddot{\Phi}_\nu}$, respectively. If the hopping time of the received frequency hopping signal is relatively long compared with T_s, then $N \to \infty$. Thus, the exponential summation in $H_{\mathrm{A},0}(\omega)$ equals to the summation of

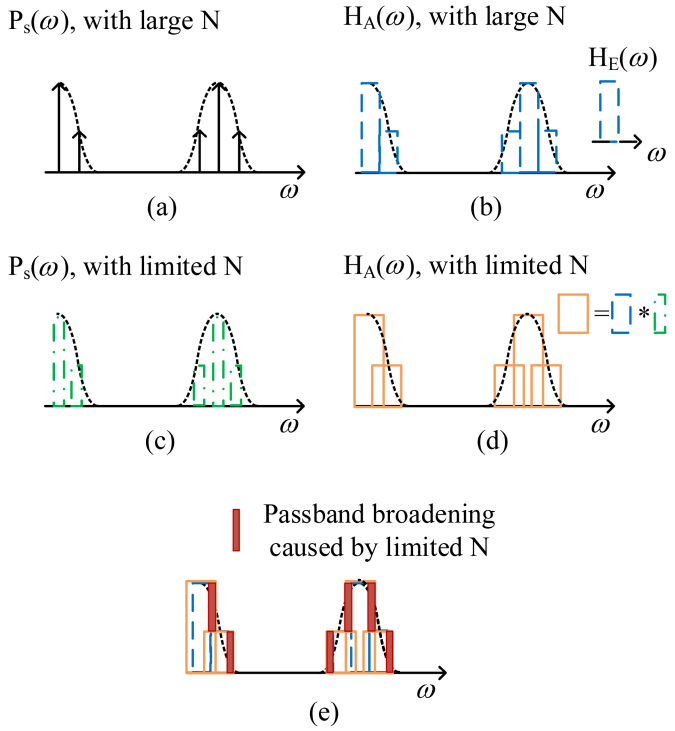

Fig. 2. The schematic of the broadening of the equivalent system response with limited number of sampling points, N.

delta function [2], and $H_{\mathrm{A},0}(\omega)$ becomes

$$H_{\mathrm{A},0}(\omega)=2\alpha\cdot I_0\cdot\sum_{n=0}^{\infty}\left\{\delta\left(\omega-n\frac{2\pi}{T_{\mathrm{s}}}\right)\cdot G'(\omega)*H_{\mathrm{E}}(\omega)\right\}. \tag{5}$$

From (5), if the frequency hopping signal holds its carrier frequency for a relatively long time, the receiving passband is the summation of $H_{\mathrm{E}}(\omega)$ moved to $\omega=n\frac{2\pi}{T_{\mathrm{s}}}$ with the coefficients determined by $G'(\omega)$, which is identical to the analysis in [17], [16]. However, if the frequency hopping signal changes its carrier frequency rapidly and therefore N is limited, the summation of exponential terms in $H_{\mathrm{A},0}(\omega)$ cannot be treated as the summation of delta functions. Thus, the receiving passband is determined by the summation of the convolution of $H_{\mathrm{E}}(\omega)$ and peaks generated by $\sum_{n=0}^{N}e^{-j\omega nT_{\mathrm{s}}}$ in the expression of $H_{\mathrm{A},0}(\omega)$. The smaller N is, the broader the peaks are. Thus, the equivalent system frequency response to receive frequency hopping signals is broadened. The schematic of the shaped optical pulses, $P_{\mathrm{s}}(\omega)$ and the equivalent system response, $H_{\mathrm{A}}(\omega)$ with infinity and limited N are depicted in Fig. 2(a)–(d). The passbands of $H_{\mathrm{A}}(\omega)$ with infinity and limited N are depicted together in Fig. 2(e) as a comparison, and the broadened passband is shown in red. The limited N causes the passband distortion, and the passband is broadened on both edges with the amount caused by the width of the peaks. For frequency hopping signal with fixed hopping speed, N can be increased by utilizing ADCs with smaller sampling period of T_{s}. Therefore, the passband broadening in receiving fast hopping signals can be released. Thus, the hopping speed can be improved by using high-speed optical switches to shorten the tuning time of the shaped optical pulses, and by using ADC with higher sampling rate to fasten the rebuilding of the equivalent system response.

B. Receiving Linearity

The receiving linearity of the proposed frequency hopping receiver is mainly limited by the MZM, since the non-linearity of the electric end can be neglected when a signal enters the electric end with very small power. Specially, the non-linearity of the proposed receiver is mainly caused by the thrid-order distortions (IMD3) introduced by the MZM, because the MZM is biased at quadrature point and the even order distortions are suppressed. The spurious free dynamic range (SFDR) is defined as the power of the fundamental tone to the highest power of detectable distortions, and in this case, the power of the IMD3. To investigate the SFDR of the proposed frequency hopping receiver, the power of FT and IMD3 are derived. With a two-tone RF signal, the output optical power of the MZM is

$$\begin{aligned}I_{\mathrm{out}}(t)&=\frac{1}{2}\cdot p_{\mathrm{s}}(t)\cdot\left\{1+\cos\left[\frac{2\pi}{\mathrm{V}_\pi}(\mathrm{V_{DC}}+\mathrm{V_{RF_1}}+\mathrm{V_{RF_2}})\right]\right\}\\&=\frac{1}{2}\cdot p_{\mathrm{s}}(t)\cdot\left\{1+\cos\left[2\pi\frac{V_{\mathrm{DC}}}{V_\pi}+2\pi\frac{V_{\mathrm{RF}}}{V_\pi}\right.\right.\\&\quad\left.\left.\cdot[\sin(\omega_1\mathrm{t})+\sin(\omega_2\mathrm{t})]\right]\right\},\end{aligned} \tag{6}$$

where V_π is the half-wave voltage, and ω_{i} is the angular frequency of the received two-tone signals. With Bessel functions, the output optical intensity of the quadrature-biased MZM can be simplified as [23],

$$\begin{aligned}I_{\mathrm{out}}(t)&=\frac{1}{2}\cdot p_{\mathrm{s}}(t)+\frac{1}{2}\cdot p_{\mathrm{s}}(t)\\&\cdot\left\{2J_0\left(2\pi\frac{V_{\mathrm{RF}}}{V_\pi}\right)\cdot J_1\left(2\pi\frac{V_{\mathrm{RF}}}{V_\pi}\right)\cdot[\sin(\omega_1\mathrm{t})+\sin(\omega_2\mathrm{t})]\right.\\&+2J_1\left(2\pi\frac{V_{\mathrm{RF}}}{V_\pi}\right)\cdot J_2\left(2\pi\frac{V_{\mathrm{RF}}}{V_\pi}\right)\cdot[\sin(2\omega_1+2\omega_2)\\&+\sin(2\omega_1-\omega_2)+\sin(\omega_1+2\omega_2)+\sin(2\omega_2-\omega_1)]\\&+2J_0\left(2\pi\frac{V_{\mathrm{RF}}}{V_\pi}\right)\cdot J_3\left(2\pi\frac{V_{\mathrm{RF}}}{V_\pi}\right)\\&\left.\cdot[\sin(3\omega_1 t)+\sin(3\omega_2 t)]\right\}.\end{aligned} \tag{7}$$

The optical power of the FT and IMD3 are expressed in the first and second item in the braces in (7), respectively. Thus, the SFDR of the quadrature-biased receiver is

$$\begin{aligned}\mathrm{SFDR}&=2\sin^2\left(2\pi\frac{V_{\mathrm{DC}}}{V_\pi}\right)\\&\cdot J_1^2\left(2\pi\frac{V_{\mathrm{RF},0}}{V_\pi}\right)\cdot J_2^2\left(2\pi\frac{V_{\mathrm{RF},0}}{V_\pi}\right)-N.\end{aligned} \tag{8}$$

N denotes the normalized noise floor in dBm/Hz, and $V_{\mathrm{RF},0}$ is the received RF amplitude that equals the power of IMD3 and N. The SFDR can be obtained by measuring the voltage of the fundamental tone at the ADC output until the IMD3 rises from

the noise floor. It's worthy to note that since IMD3 is affected by V_π, unlike in other proposals, the SFDR of the proposed frequency hopping receiver at different receiving frequencies varies since the half-wave voltage of MZM varies at different frequencies [19]. Using components with higher linearity in the optical-electronic link and adopting non-linearity cancellation methods [20] can improve the receiving linearity.

C. RF Gain

The RF gain of the proposed receiver is investigated based on the microwave photonics link analysis. As shown in Fig. 1, the received RF signals are modulated by the shaped optical pulse train $p_{\mathrm{s}}(t)$ through a quadrature-biased MZM working on the small signal condition. In this case, the response of MZM, $h_{\mathrm{M}}(t)$ is regarded as linear. The output optical intensity containing the received frequency hopping signals, denoted by $y(t)$, is

$$I_{\mathrm{out}}(t) = \frac{1}{2}p_{\mathrm{s}}(t) + \frac{1}{2}p_{\mathrm{s}}(t)\cdot\left[h_{\mathrm{M}}(t) * y(t)\right]. \tag{9}$$

The modulated optical pulses are detected and digitized with the period of T_s afterwards, and the digitized result is

$$v[n] = \left\{\frac{1}{2}p_{\mathrm{s}}(t) * h_{\mathrm{E}}(t) + \frac{1}{2}p_{\mathrm{s}}(t)\cdot\left[h_{\mathrm{M}}(t) * y(t)\right] * h_{\mathrm{E}}(t)\right\}\Big|_{t=nT_{\mathrm{s}}} \tag{10}$$

The frequency hopping signals are modulated in the second term in the braces, denoted as $v_1[n]$. According to [17], [21], it can be derived as

$$\begin{aligned} v_1[n] &= \frac{1}{2}p_{\mathrm{s}}(t)\cdot\left[h_{\mathrm{M}}(t) * y(t)\right] * h_{\mathrm{E}}(t)\Big|_{t=nT_{\mathrm{s}}} \\ &= \frac{1}{2}h_{\mathrm{M}}(t) * y(t) * \left[p_{\mathrm{s}}(-t)\cdot h_{\mathrm{E}}(t)\right]\Big|_{t=nT_{\mathrm{s}}}, \\ V_1(\omega) &= \frac{1}{2\pi}\cdot\left\{\frac{1}{2}H_{\mathrm{M}}(\omega)\cdot Y(\omega)\cdot\left[P_{\mathrm{s}}(\omega) * H_{\mathrm{E}}(\omega)\right]\right\} * S_\delta(j\omega). \end{aligned} \tag{11}$$

where the function denoted by the capital letter is the Fourier transform of the function denoted by the corresponding lower-case. $S_\delta(j\omega)$ is the sampling function. To receive the frequency hopping signal whose carrier frequency is $\omega_{\mathrm{c,n}}$, the optical switch in Fig. 1 should be switched to the path that has the delay of τ_{n} that corresponds to the receiving passband at $\omega_{\mathrm{c,n}}$. Therefore, the $H_{\mathrm{A},0}(\omega)$ in (4) is moved to $\omega = \omega_{\mathrm{c,n}}$ for signal receiving. Then the digitized frequency hopping signal observed in the frequency domain can be expressed as

$$\begin{aligned} V_{1,\omega_{\mathrm{c,n}}}(\omega) = {} & \frac{I_0}{2\pi}H_{\mathrm{M}}\left(\omega_{\mathrm{c,n}}\right)\cdot\alpha\left(\omega_{\mathrm{c,n}}\right)\cdot Y(\omega)\cdot S_\delta(j\omega) * \\ & \left\{\left[\sum_{n=0}^{N-1}\left[e^{-j\omega nT_{\mathrm{s}}}\cdot G'(\omega) * \delta\left(\omega - \frac{\tau_n}{\ddot{\Phi}_\nu}\right)\right] * H_E(\omega)\right]\right. \\ & \left. + \left[\sum_{n=0}^{N-1}\left(e^{-j\omega nT_s}\cdot G'(\omega) * \delta(\omega)\right) * H_E(\omega)\right]\right\} \end{aligned} \tag{12}$$

Equation (12) indicates that the digitized signal has AC component, as the first item in the braces, and DC component, as the second item in the braces. Since the DC component in the sampling spectral window indicates that the signal whose frequency is the integer multiples of the sampling rate, it is filtered out before procession. Only the AC component in (12) is considered in the investigation of the receiving RF gain. Since $G'(\omega)$ in (12) is determined by the optical spectrum of MLL and the dispersion value introduced by the SMF in Fig 1, its maximum, which corresponds to the maximum receiving gain of the receiving passband, is determined by the optical power, I_0. The gain introduced by $H_{\mathrm{E}}(\omega)$ is denoted as K in the calculation of RF gain. Then the RF gain,denoted as G_{RF}, can be expressed as

$$G_{\mathrm{RF}}\left(\omega_{\mathrm{c,n}}\right) = \frac{I_0\cdot K}{2\pi}\left|H_{\mathrm{M}}\left(\omega_{\mathrm{c,n}}\right)\right|\cdot\alpha\left(\omega_{\mathrm{c,n}}\right) \tag{13}$$

In (13), $\left|H_{\mathrm{M}}(\omega_{\mathrm{c,n}})\right|$ is the amplitude response of the MZM at $\omega = \omega_{\mathrm{c,n}}$, and its value varies as the receiving frequency $\omega_{\mathrm{c,n}}$ changes because of the ripples and decline introduced by the MZM frequency response. $\alpha(\omega_{\mathrm{c,n}})$, as defined in (1), is the visibility of the optical interference with the delay difference corresponding to the receiving angular frequency of $\omega_{\mathrm{c,n}}$. Since the switching of optical switches introduces optical power or polarization fluctuations between two interference arms, α is a function of $\omega_{\mathrm{c,n}}$. The optical power I_0, and the gain introduced by the electric end, K, are considered as constants during the tuning of receiving frequencies.

Equation (13) indicates that the RF gain increases with higher optical power I_0, higher MZM response $|H_{\mathrm{M}}(\omega)|$, larger visibility in optical interference $\alpha(\omega)$, and larger gain of electric end K. In order to improve the visibility of the optical interference, precise control methods on the optical power and polarization state [22] are needed [3].

D. Signal-to-Noise Ratio

The analysis in Section II, C implies that the RF gain changes as the receiving frequency changes due to $\left|H_{\mathrm{M}}(\omega)\right|$ and $\alpha(\omega)$. The changing of the receiving gain in different receiving frequency affects the average signal-to-noise ratio (SNR) of the received frequency hopping signals. To calculate the average SNR, all possible receiving passbands should be considered.

A time interval, denoted as T_{total}, is taken into consideration when all the frequencies in the frequency hopping pattern are used as the carrier frequency for the first time. If the received frequency hopping signal has even amplitude of 1 regardless of its carrier frequency, the received signal amplitude at $\omega = \omega_{\mathrm{c,n}}$ is

$$v_{1,\omega_{\mathrm{c,n}}} = G_{\mathrm{RF}}\left(\omega_{\mathrm{c,n}}\right) = \frac{I_0\cdot K}{2\pi}\left|H_{\mathrm{M}}\left(\omega_{\mathrm{c,n}}\right)\right|\cdot\alpha\left(\omega_{\mathrm{c,n}}\right). \tag{14}$$

Within T_{total}, the probability intensity function of the carrier frequency $\omega_{\mathrm{c,n}}$ is denoted as $f_{\omega_{\mathrm{c,n}}}(t)$. Thus, the probability of using $\omega_{\mathrm{c,n}}$ as the carrier frequency is

$$P_{\omega_{\mathrm{c,n}}} = \int_0^{T_{\mathrm{total}}} f_{\omega_{\mathrm{c,n}}}(t)dt. \tag{15}$$

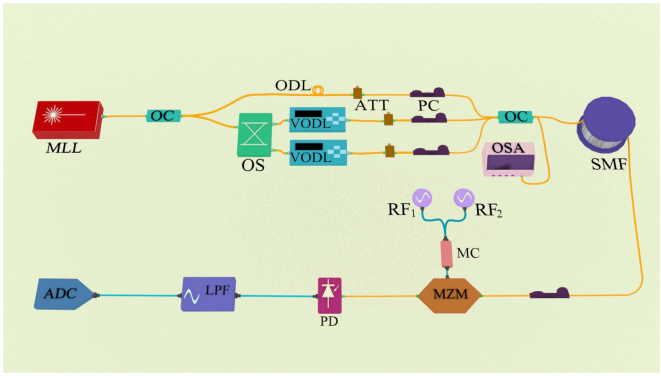

Fig. 3. The setup of the verification experiments. MLL: mode-locked laser; OC:optical coupler; OS: optical switch; ODL: optical delay line;: VODL: variable optical delay line; ATT: attenuator; PC: polarization controller; SMF: single mode fiber; RF: radio-frequency sources; MC: microwave coupler; MZM: Mach-zehnder modulator; PD: photodiode; LPF: low-pass-filter; ADC: analog-to-digital convertor; OSA: optical spectrum analyzer.

Within the period of T_{total}, the average received signal amplitude, denoted as $\overline{|v_{1,\omega_c}|}$, is

$$\begin{aligned}\overline{|v_{1,\omega_c}|} &= \frac{\sum_{n=1}^{num} P_{\omega_{c,n}} \times T_{\text{total}} \times |v_{1,\omega_{c,n}}|}{T_{\text{total}}} \\ &= \sum_{n=1}^{num} \left[\int_0^{T_{\text{total}}} f_{\omega_{c,n}}(t)dt \times |v_{1,\omega_{c,n}}| \right], \end{aligned} \tag{16}$$

where num is the total number of receiving passbands in the frequency hopping pattern. Suppose the noise power, P_{noise}, remains unchanged during T_{total}. Then the average SNR is

$$\begin{aligned}\overline{SNR} &= \frac{\sum_{n=1}^{num} \overline{|v_{1,\omega_c}|}^2}{P_{\text{noise}}} \\ &= \frac{{I_0}^2 \cdot K^2}{4\pi^2 \times P_{\text{noise}}} \\ &\quad \times \sum_{n=1}^{num} \left[\int_0^{T_{\text{total}}} f_{\omega_{c,n}}(t)dt \times \left| H_{\text{M}}(\omega_{c,n}) \right| \cdot \alpha(\omega_{c,n}) \right]^2 \end{aligned} \tag{17}$$

If the frequencies in the frequency hopping pattern are uniformly distributed, the probability intensity function of frequency $\omega_{c,n}$ is $f_{\omega_{c,n}}(t) = \frac{1}{num}$. Then with (17), the average SNR with uniformly distributed frequency hopping pattern, denoted as $\overline{SNR_u}$ is

$$\overline{SNR_u} = \frac{{I_0}^2 \cdot K^2 \times \sum_{n=1}^{num} \left[\left| H_{\text{M}}(\omega_{c,n}) \right| \cdot \alpha(\omega_{c,n}) \right]^2}{4\pi^2 \times num^2 \times P_{\text{noise}}}. \tag{18}$$

III. Experimental Verification

To verify the theoretical analysis above, experiments on the receiving linearity and receiving gain have been conducted based on the experimental setup shown in Fig. 3. The MLL with the repetition rate of 250 MHz provides the optical pulses train in the experiments. In optical interference, the upper arm is fixed with optical delay line (ODL), ATT and PC to compensate for

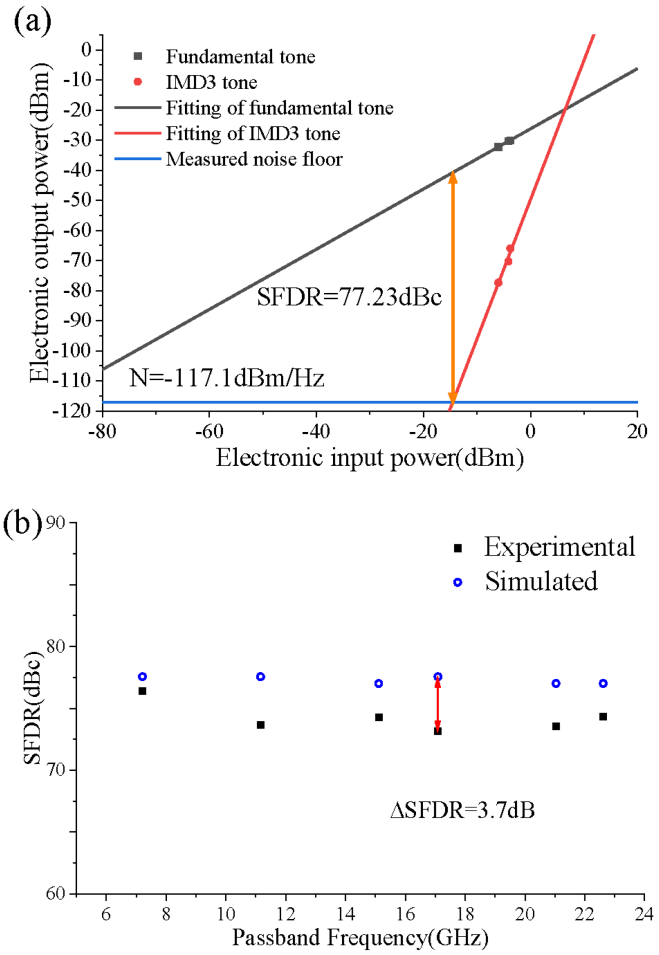

Fig. 4. Experimental results on receiving linearity. (a) measured SFDR with receiving frequency of 7.21 GHz and (b) measured and simulated SFDR with the receiving frequencies from 7 GHz to 21 GHz.

the length, the optical loss and polarization in the lower arm. By switching the optical switch, the time difference between the two interference arms is swiftly changed, and the frequency hopping signal between two frequencies can be received. The variable optical delay lines (VODL) are used in the lower arm to continuously tune the time difference between the optical interference arms so that all passbands within the working bandwidth of the frequency hopping receiver can be investigated. Using a 1:9 optical coupler (OC), 10% of the optical power of the optical pulses after interference is captured by an optical spectrum analyzer (OSA,YOKOGAWA 6370D). The rest 90% of the optical pulses are sent into SMF to conduct frequency-to-time mapping. The length of the SMF is ~9.9 km, which introduces the Φ_ν of $\sim 1.22 \times 10^3 ps^2$. After interference and frequency-to-time mapping, the shaped optical pulses are sent into a 40 GHz MZM with the adjusted polarization state identical to that of the MZM's to receive the test signals that are generated by two RF sources and coupled by a DC-40 GHz microwave coupler (MC). The two RF sources used in the experiments are Agilent N5183B and Rohde & Schwarz SMF 100 A, both can generate microwave signals up to 40 GHz. The bandwidth of PD, LPF and ADC is 1 GHz, 167 MHz and 2 GHz, respectively.

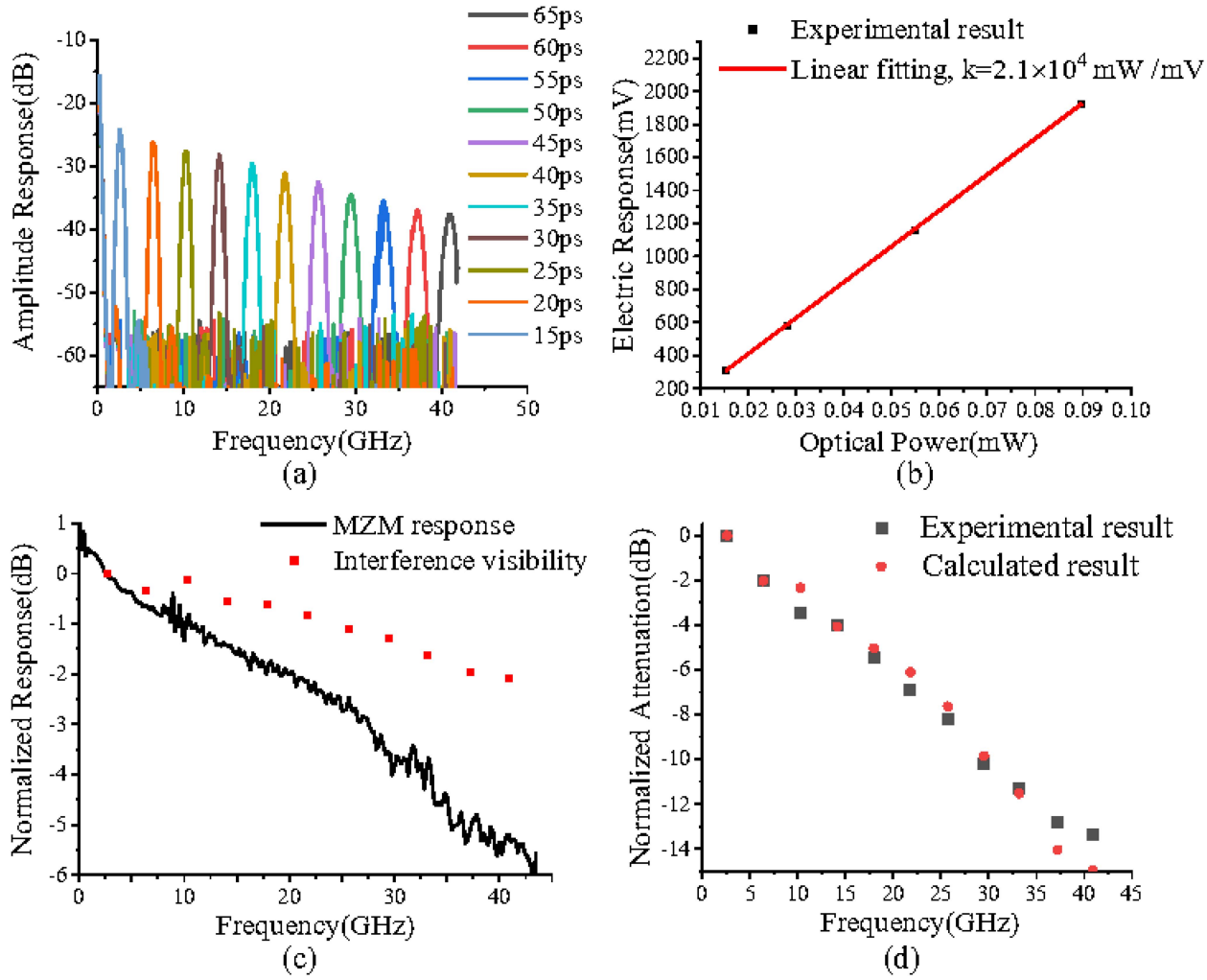

Fig. 5. The results of the experiments on RF gain, (a) the equivalent system response with different delays; (b) the experimental result of the PD responsibility; (c) the MZM amplitude frequency response $\left|H_M(\omega)\right|$, and the visibility of the shaped optical spectrum, $\alpha(\omega)$, that is extracted from the OSA; (d) the RF gain calculated theoretically and the experimental results.

Thus, the bandwidth of $h_E(t)$ is 167 MHz. The sampling rate of the ADC is identical to the repetition rate of the MLL, which is 250MS/s.

A. Receiving Linearity

To test the receiving linearity, both RF sources are activated. Fig. 4(a) shows the power of the fundamental tone and the IMD3 tone with the increase of input RF power from -10 dBm to 0 dBm to satisfy the small signal condition for the MZM. The receiving frequency is 7.21 GHz, and the test signals are 7.199 GHz and 7.221 GHz, respectively. The IMD3 power increases with the slope of 3 as the power of the fundamental tone increases linearly. The power of the FT is -39.87 dBm when the IMD3 equals the normalized noise floor of -117.1 dBm/Hz. Thus, the SFDR at 7.21 GHz is 77.23 dBc.

Then the VODL is tuned with the step of 5 ps to investigate SFDR variations in different receiving frequencies. After the tuning of VODL, only one RF source is activated at first to sweep within the working bandwidth of DC-40 GHz to determine the current receiving frequency. With a known receiving frequency at f_c, both of the RF sources are activated and set to $f_c \pm 11$ MHz to test the power of IMD3. Fig. 4(b) shows the measured SFDRs of the receiving passbands from 7 GHz to 23 GHz, and the variation is below 3.2 dB. This variation is caused by the change of V_π with the tuning of the receiving frequency [19], as the coefficient of $\sin^2(2\pi \frac{V_{DC}}{V_\pi})$ in (8) is related to V_π. The theoretical SFDR at different receiving frequencies are calculated through (8) by substituting the amplitude of the two-tone test signal and V_π of 10.8 V. The difference between the simulated and tested SFDR is less than 3.7 dB, as illustrated in Fig. 4(b). This is caused by the changing of V_π at different frequencies, and the frequency-dependent RF gain of the receiving passband, as the noise distorts the FT and IMD3 power more in the passbands with lower gain.

B. RF Gain

According to the theoretical analysis and (13), the RF gain of the proposed frequency hopping receiver is determined by the optical power, the response of MZM, the visibility of the optical interference and the gain introduced by the electric end.

TABLE I
THE COMPARISON BETWEEN THE PROPOSED FREQUENCY HOPPING RECEIVER AND OTHER SCHEMES

Reference	Year	Frequency hopping range	Frequency hopping time	SFDR	RF gain
[10]	2016	DC-7.5GHz	20ns	107dBc	/
[24]	2017	1.1&2.1GHz	0.2ns	/	-30dB@1.1GHz
[2]	2018	DC-12GHz	1.73ns	/	-20dB@4.65GHz
This work	2023	2-40GHz	250ns [4]	77.23dBc	-24dB@2.44GHz

To verify the theoretical analysis of the RF gain, an experiment is carried out using the schematic in Fig. 3.

By setting VODL to different values, the receiving frequency is tuned. For a fixed delay corresponding to the receiving frequency of $\omega_{c,n}$, the optical spectrum after interference is captured by the OSA to extract $\alpha(\omega_{c,n})$. Then only one RF source is activated with fixed power of 0 dBm to sweep the frequency range once at a time. The equivalent system amplitude-frequency response at the swept frequency can be obtained from the output of the ADC. Then the RF gain of the passband at $\omega = \omega_{c,n}$ can be extracted from the equivalent system response. Fig. 5(a) shows the equivalent system response under different delays. To theoretically calculate the RF gain according to (13), the gain of the electric end, K, and the response of the MZM, $\left|H_M(\omega)\right|$ are tested. The gain of the electric end is mainly introduced by the PD with trans-impedance amplifier. The response of the PD is tested by recording the output voltage of PD when inputting a continuous optical wave with known power. The responsibility of the PD used in the experiment is $K = 2.1 \times 10^4$ mW/mV, and the test result is depicted in Fig. 5(b). The amplitude response of MZM tested by a commercial vector network analyzer is shown in Fig. 5(c), together with the visibility of the optical spectrum after interference, $\alpha(\omega)$. Using $\left|H_M(\omega)\right|$, $\alpha(\omega)$, and K tested in the experiments, the theoretical RF gain is calculated through (13), and shown in Fig. 5(d). As a comparison, the RF gain extracted from Fig. 5(a) is also depicted in Fig. 5(d) as the gains in experiment. The difference between the theoretical and the experimental result of the RF gain is less than 2 dB. Thus, it proves the correctness of the theoretical analysis in Section II-C.

With the assumption of utilizing uniformly-distributed frequency hopping pattern, the average SNR is expressed in (19). Substituting the measured RF gain of different passbands in Fig. 5(d), the average SNR is

$$\begin{aligned}\overline{SNR_{\mathrm{u,exp}}} &= 10 \times log_{10}\left(\frac{0.0128}{121 \times P_{\mathrm{noise}}}\right) \\ &= -39.75 \text{ dB } - P_{\mathrm{noise,\,dB}} \end{aligned} \tag{19}$$

There are plenty of methods to improve the RF gain, and the average SNR of the proposed frequency hopping receiver can be improved consequently. For example, using a narrow-band electric amplifier placed after the PD in Fig. 3 can improve the SNR effectively.

Eventually, for the purpose of comparison, Table I collects the frequency hopping range, the hopping speed together with the SFDR and RF gain of the proposed receiver and other microwave photonics schemes that are suitable for frequency hopping receiving. The proposed receiver extends the frequency hopping range from X band to Ka band with a hopping time of 250 ns, which provides enhanced anti-interference and anti-interception performances [1], and its RF gain is similar to other schemes. For the moderate SFDR, it can be improved by using balanced PD to eliminate the common-mode interference, and other linearization methods [20].

IV. CONCLUSION

The receiving performance, including the hopping speed, the receiving linearity and RF gain of the previously proposed frequency hopping receiver based on interference and frequency-to-time mapping have been theoretically analyzed, and the latter two have been experimentally tested. With high frequency hopping speed, the equivalent system response to receive the corresponding signal is broadened compared with the designed passband, and the suppression on noise and interference is degraded. Utilizing MLL and ADC with higher reprtition/sampling rate can release the degradation. The receiving linearity of the proposed frequency hopping receiver is mainly limited by the IMD3 introduced by the quadrature-biased MZM when the signal entering the electric end is small. The SFDR of the passband at 7.21 GHz is 77.23dBc, and the variance on SFDR of different receiving frequencies from 7 GHz to 21 GHz is less than 3.2 dB. The simulated SFDR is calculated from the test signal power used in the experiment according to the theoretical analysis, and it agrees well with the experimental SFDR with the difference of less than 3.7 dB. The fluctuation in SFDR is introduced by the shifting of V_π and the frequency-dependent RF gain. The RF gain of different passbands varies due to the uneven amplitude frequency response of the MZM, and the change of interference visibility with various time difference. The RF gain of the receiving passbands at frequencies from 2 GHz to 40 GHz are tested in the experiments, and calculated according to the theoretical analysis and the parameters tested in the experiments. The difference of the theoretical and experimental results is less than 2 dB. The variance on RF gain at different receiving frequencies has the impact on the average SNR when receiving frequnecy hopping signals. With larger RF gains, the average SNR can be increased.

ACKNOWLEDGMENT

This paper was produced by the IEEE Publication Technology Group. They are in Piscataway, NJ.

REFERENCES

[1] J. Bird and E. Felstead, "Antijam performance of fast frequency-hopped M-ary NCFSK–an overview," *IEEE J. Sel. Areas Commun.*, vol. 4, no. 2, pp. 216–233, Mar. 1986.

[2] P. Li, W. Pan, X. Zou, B. Lu, and L. Yan, "Fast tunable photonic single-bandpass RF filter with multiple arbitrary switching flat-top passbands," *J. Lightw. Technol.*, vol. 36, no. 19, pp. 4583–4590, Oct. 2018.
[3] Y. Sun, S. Wang, J. Chen, and G. Wu, "Interference and frequency-to-time mapping based high anti-jamming and anti-interception frequency hopping receiving," *Opt. Exp.*, vol. 29, no. 17, pp. 26486–26495, 2021.
[4] R. A. Roberts and R. A. Gabel, *Signals and linear systems*, Hoboken, NJ, USA: Wiley, 1991.
[5] H. J. Kim and A. M. Weiner, "Intermodulation distortion of a comb-based RF photonic filter using balanced detection," *IEEE Photon. Technol. Lett.*, vol. 27, no. 23, pp. 2477–2480, Dec. 2015.
[6] D. H. Mahrof, E. A. M. Klumperink, Z. Ru, M. S. Oude Alink, and B. Nauta, "Cancellation of OpAmp virtual ground imperfections by a negative conductance applied to improve RF receiver linearity," *IEEE J. Solid-State Circuits*, vol. 49, no. 5, pp. 1112–1124, May 2014.
[7] L. Peng and H. Ma, "Design and implementation of software-defined radio receiver based on blind nonlinear system identification and compensation," *IEEE Trans. Circuits Syst. I. Regular Papers*, vol. 58, no. 11, pp. 2776–2789, Nov. 2011.
[8] R. Winoto and B. Nikolic, "A highly reconfigurable 400–1700MHz receiver using a down-converting sigma-delta A/D with 59-dB SNR and 57-dB SFDR over 4-MHz bandwidth," in *Proc. 2009 Symp. VLSI Circuits*, 2012, pp. 142–143.
[9] R. Helkey, J. C. Twichell, and C. Cox, "A. down-conversion optical link with RF gain," *J. Lightw. Technol.*, vol. 15, no. 6, pp. 956–961, Jun. 1997.
[10] H. J. Kim, D. E. Leaird, and A. M. Weiner, "Rapidly tunable dual-comb RF photonic filter for ultrabroadband RF spread spectrum applications," *IEEE Trans. Microw. Theory Techn.*, vol. 64, no. 10, pp. 3351–3362, Oct. 2016.
[11] H. J. Kim, D. E. Leaird, A. J. Metcalf, and A. M. Weiner, "Comb-based RF photonic filters based on interferometric configuration and balanced detection," *J. Lightw. Technol.*, vol. 32, no. 20, pp. 3478–3488, Oct. 2014.
[12] M. E. Manka, "Microwave photonics for electronic warfare applications," in *Proc. IEEE Int. Topical Meeting Microw. Photon.*, 2008, pp. 275–278.
[13] J. Mora et al., "Photonic microwave tunable single-bandpass filter based on a Mach-Zehnder interferometer," *J. Lightw. Technol.*, vol. 24, no. 7, pp. 2500–2509, Jul. 2006.
[14] V. Torres-Company, D. E. Leaird, and A. M. Weiner, "Dispersion requirements in coherent frequency-to-time mapping," *Opt. Exp.*, vol. 19, no. 24, pp. 24718–24729, 2011.
[15] F. Su, G. Wu, and J. Chen, "Photonic analog-to-digital conversion with equivalent analog prefiltering by shaping sampling pulses," *Opt. Lett.*, vol. 41, no. 12, pp. 2779–2782, 2016.
[16] S. Wang, G. Wu, Y. Sun, and J. Chen, "Principle of integrated filtering and digitizing based on periodic signal multiplying," *Opt. Lett.*, vol. 44, no. 7, pp. 1766–1769, 2019.
[17] F. Su, G. Wu, L. Ye, R. Liu, X. Xue, and J. Chen, "Effects of the photonic sampling pulse width and the photodetection bandwidth on the channel response of photonic ADCs," *Opt. Exp.*, vol. 24, no. 2, pp. 924–934, 2016.
[18] S. Wang, G. Wu, F. Su, and J. Chen, "Simultaneous microwave photonic analog-to-digital conversion and digital filtering," *IEEE Photon. Technol. Lett.*, vol. 30, no. 4, pp. 343–346, Feb. 2018.
[19] T. Sutili and E. Conforti, "Optical modulator half-wave voltage measurement using opposite-phase sine waves," *J. Lightw. Technol.*, vol. 34, no. 9, pp. 2152–2157, May 2016.
[20] G. Liu et al., "Integrated microwave photonic spectral shaping for linearization and spurious-free dynamic range enhancement," *J. Lightw. Technol.*, vol. 39, no. 24, pp. 7551–7562, Dec. 2021.
[21] Y. Sun, S. Wang, J. Chen, and G. Wu, "Fast and large-range frequency hopping receiving based on simultaneous photonic filtering and digitizing," *Opt. Lett.*, vol. 46, no. 4, pp. 749–752, 2021.
[22] K. H. Wanser and N. H. Safar, "Remote polarization control for fiber-optic interferometers," *Opt. Lett.*, vol. 12, no. 3, pp. 217–219, 1987.
[23] H. B.Kolner, and D. W. Dolfi, "Intermodulation distortion and compression in an integrated electrooptic modulator," *Appl. Opt.*, vol. 26, no. 17, pp. 3676–3680, 1987.
[24] J. Ge and M. P. Fok, "Optically controlled fast reconfigurable microwave photonic dual-band filter based on nonlinear polarization rotation," *IEEE Trans. Microw. Theory Techn.*, vol. 65, no. 1, pp. 253–259, Jan. 2017.